Received: 11 October 2023 | Revised: 2 January 2024 | Accepted: 21 March 2024

DOI: 10.1002/jrs.6671

RESEARCH ARTICLE

Journal of RAMAN SPECTROSCOPY WILEY

Dual coherent anti-Stokes Raman scattering microscopy across the vibrational spectrum enabled by single pump optically synchronised oscillators and spectral focusing

Dominykas Gudavičius[1,2] | **Lukas Kontenis**[1] | **Wolfgang Langbein**[2]

[1]Light Conversion, Vilnius, Lithuania

[2]School of Physics and Astronomy, Cardiff University, Cardiff, UK

Correspondence
Wolfgang Langbein, School of Physics and Astronomy, Cardiff University, The Parade, Cardiff CF24 3AA, UK.
Email: langbeinww@cardiff.ac.uk

Funding information
European Union's Horizon 2020, Grant/Award Number: 812992

Abstract

Coherent anti-Stokes Raman scattering microscopy probing two independently selectable vibrational frequencies across the vibrational spectrum is demonstrated. A one-box femtosecond laser source provides three synchronised 100–200 fs pulses of 77 MHz repetition rate, one at a fixed wavelength of 1025 nm from an Yb oscillator and two independently tuneable ones, over 680–960 nm and 960–1300 nm, respectively, from two optically synchronised parametric oscillators. Combined with spectral focusing, the source allows addressing the fingerprint, cell silent and C–H stretch vibrational regions simultaneously, avoiding the motion artefacts seen in sequential imaging. We demonstrate the microscopy method on water/heavy water/oil emulsions, plastic beads and deuterated lipids inside cells.

KEYWORDS

CARS, microscopy, optical parametric oscillator, Raman, spectral focusing

1 | INTRODUCTION

Coherent Raman scattering (CRS) allows chemical imaging microscopy using the vibrational response of the chemical components of the sample without using fluorescent dyes.[1–4] In a nutshell, an optical excitation that is intensity modulated at the vibrational frequency is driving molecular vibrations due to the dependence of the molecular polarisability on the vibrational coordinate. The driven vibrations are in turn modulating the polarisability, creating sidebands of the optical excitation fields. These sidebands are the CRS and their amplitude and phase report the vibrational spectrum of the medium. There are many different ways to design the optical excitation and to detect these sidebands, with different advantages and drawbacks.[1,4] A simple scheme uses two synchronised optical pulses, the pump pulse and the longer wavelength Stokes pulse, with a frequency difference given by the vibrational frequency of interest. To achieve high intensities while keeping the average power below sample damage, pulses of picosecond duration, comparable with the typical vibrational coherence time in condensed matter, with high repetition rates in the 1–100 MHz range to allow a high pixel rate up to these values, are used. The duty cycle in the 10^{-4} to 10^{-6} range enables achieving peak intensities of the order of 10^{11}–10^{12} W/cm^2 when focussed by a microscope objective, suitable for efficient CRS generation just below typical saturation levels[5] around 10^{13} W/cm^2, for average powers of tens of milliwatts and typical diffraction limited sub-micron focus sizes.

The high-frequency sideband of the pump, called coherent anti-Stokes Raman scattering (CARS), can be detected free of excitation background. CARS is also created by purely electronic non-linearities such as the Kerr effect, as well as by non-resonant responses of higher frequency vibrations, providing a background to the resonant response. Detecting the CARS power therefore shows asymmetric resonance lineshapes on a background, complicating the interpretation of the contrast. To retrieve a signal linear in the concentration of the chemical components, the complex susceptibility can be determined by phase retrieval using the causality of the response and the measured dependence on the vibrational frequency.[6–8] Alternatively, the CARS field can be directly detected interferometrically.[9,10]

A simple way to isolate the resonant response in CARS is to measure at two vibrational frequencies simultaneously, probing the dispersive response in the presence of a strong non-resonant background, either by wavelength modulation[11] or using spectral focusing.[12,13] The latter is also able to address widely separated frequencies but not fully covering from cell silent to C–H stretch region due to laser bandwidth[12] or higher-order dispersion in the glass used.[13] For CARS dominated by resonant responses, for example, C–H vibrations in lipid droplets larger than the spatial resolution, the two frequencies can be used to target two different vibrational resonances, distinguishing, for example, deuterated from non-deuterated lipids. Dual CARS thus allows for example to measure simultaneously deuterated and non-deuterated substances, such as lipid bilayers,[14] lipid droplets,[15] or glycerol in skin.[16]

Two individual optical parametric oscillators (OPOs) have been used in the past[17,18] to provide two independently addressable vibrational frequencies. Recently, dual band CARS using Fourier-transform impulsive excitation employing a Ti:Sa oscillator and a synchronised Yb fibre laser was shown to cover both fingerprint and C–H stretch region.[19]

Here, we present a dual CARS imaging system with a spectral focusing scheme using a one-box light source integrating a femtosecond Yb oscillator and two OPOs, which covers the fingerprint, silent and CH stretching region.

2 | MATERIALS AND METHODS

2.1 | Microscope set-up

The microscope set-up developed and used is sketched in Figure 1A. The laser source (CRONUS-2P, Light Conversion) provides three output beams of Fourier-limited femtosecond pulses at 77 MHz repetition rate. The 680–960 nm OPO output was used as a pump, the 960–1300 nm OPO output as Stokes for the C–H stretch

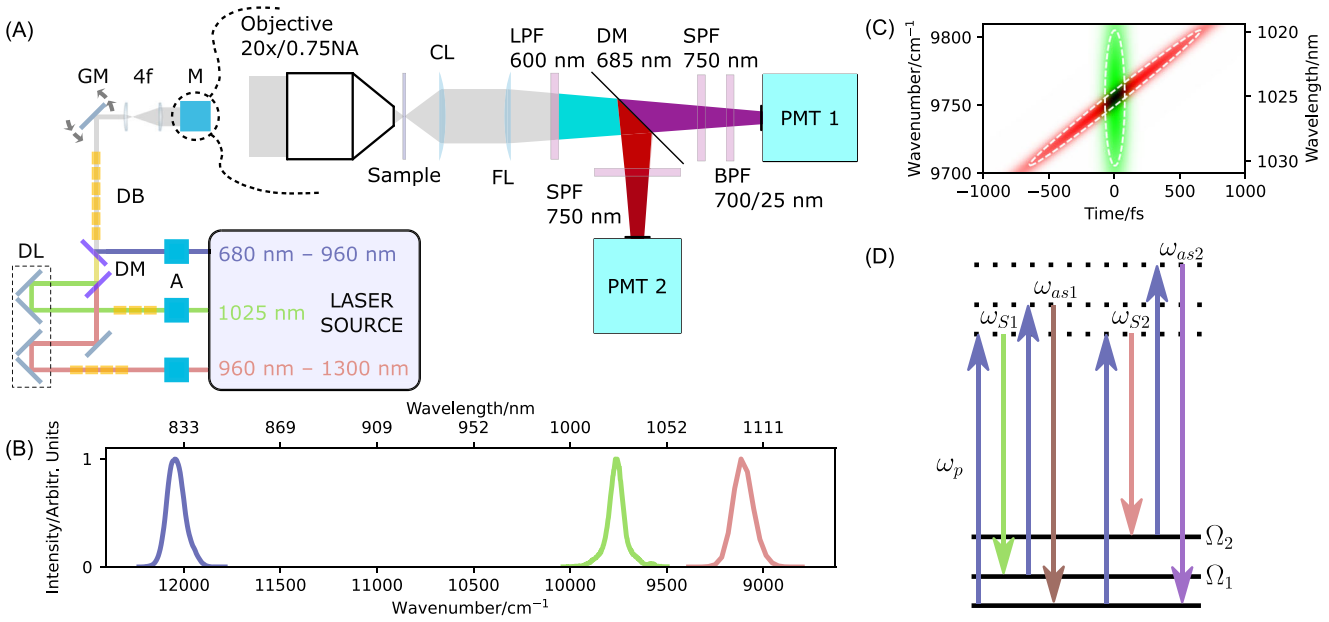

FIGURE 1 (A) Experimental set-up with the components: A, power attenuator; DL, delay line; DM, dichroic mirror; DB, dispersion block; GM, galvo mirror; 4f, relay from GM to objective back focal plane; M, microscopy rack; CL, condenser lens; FL, focusing lens; LPF, longpass filter; SPF, shortpass filter. (B) Pulse spectra used in the experiments. (C) Calculated Wigner–Ville distributions of a Fourier-limited 150 fs pulse at 1025 nm centre wavelength in green stretched to 1.3 ps in red. Dashed white line shows intensity FWHM contours. (D) Dual CARS energy level diagram.

region and the 1025 nm Yb oscillator output as Stokes for the cell-silent region. The spectral intensity full width at half maximum (FWHM) was 103 cm^{-1} for the pump at 831 nm, 121 cm^{-1} for the tuneable Stokes at 1093 nm and 78 cm^{-1} for the fixed Stokes at 1025 nm, corresponding to Fourier-limited pulse durations around 150 fs. Representative spectra are given in Figure 1B. We give frequencies in wavenumber units as commonly used in vibrational spectroscopy. Motorised power attenuators (A) consisting of a half-wave plate and a Glan–Taylor polariser were used to adjust the pulse energy of each output. The pump and the fixed Stokes beam were delayed by separate optical delay lines using linear stages (VT-80, Physik Instrumente) and silver mirror retroreflectors to overlap the pulses in time and control the instantaneous frequency difference (IFD) in spectral focusing. The fixed Stokes is combined with the tuneable Stokes by a dichroic mirror (DM) (shortpass 1030 nm, EKSMA Optics), and the pump is combined with the two using another DM (longpass 1000 nm, 87-041, Edmund Optics). Dispersion blocks (DBs) made of dense flint glass SF57 and N-SF66 (II-VI incorporated) and ZnS crystals (Castech) were added in the beam path to apply linear chirp to the pulses for spectral focusing, stretching them to picosecond duration. The DB dispersion is discussed in Appendix A. The fixed and tunable Stokes pulses passed through 100 and 160 mm N-SF66 glass, respectively, before recombination, and all pulses traversed 145 mm of SF57, 140 mm of N-SF66 and 30 mm of ZnS, resulting in a group delay dispersion (GDD) of 81,100 fs^2 for the pump, 76,300 fs^2 for the fixed Stokes and 78,200 fs^2 for the tuneable Stokes. The internal GDD control available in the CRONUS-2P for the pump and tuneable Stokes was used to fine-tune the GDD to match to one of the fixed Stokes stretching the 150 fs tuneable pump and Stokes beams to 1.42 ps and the 170 fs fixed Stokes beam to 1.26 ps. More details on the spectral focusing are given in Appendix B. The excitation beam is then deflected by galvo mirrors (GMs) (6215H, Cambridge Technology) and a 4f relay system consisting of three achromatic doublets (closely spaced pair of AC300-100-B with curved surfaces pointing at each other to reduce coma aberrations and a single AC508-200-B-ML, Thorlabs) with curved surface pointing towards the collimated beam providing 4× beam expansion of the 4 mm beam diameter (at $1/e^2$) to fill the 15 mm diameter back aperture of the excitation objective (20× 0.75 NA Plan Apo lambda, Nikon). The generated CARS along with the excitation pulses is collected by a condenser lens (LA1951-A, Thorlabs) of 25 mm focal length and 0.5 NA and is converged by a lens FL (LA1708, Thorlabs) of focal length 200 mm to about 5 mm size onto the 8 mm diameter cathodes of the photomultiplier tubes (PMTs) used to detect the CARS signal. A 600 nm longpass filter (FEL0600, Thorlabs) is used to remove second and third harmonic generation signals. The two CARS signals are separated by a DM (T685lpxr, Chroma Technology), and the excitation pulses are blocked by 750 nm shortpass filters (FES0750, Thorlabs). The silent region CARS signal S_{SR} (around 699 nm) is filtered by a 25 nm wide bandpass filter centred at 700 nm (86-658, Edmund Optics) and detected by PMT1 with an extended red multialkali photocathode (H10721-20, Hamamatsu). The PMT current is amplified by a current-to-voltage converter (C9999, Hamamatsu) with 10 MHz bandwidth and 50 kΩ transimpedance. The signal bandwidth was limited by a 100 kHz low pass filter (EF502, Thorlabs) before being digitised by a 16-bit analog to digital converter in a digital acquisition unit (PCI-6122, National Instruments). The PMT gain control was set to 1.0 V, providing a nominal gain of 2×10^6, so that 1 V signal corresponds to 6.25×10^7 photoelectrons/s. The C–H stretch signal S_{CH} (around 670 nm) is detected by PMT2 with an ultra bialkali photocathode and a photon counting circuit (H10682-210, Hamamatsu) providing TTL pulses which are counted by a counter in the digital acquisition unit. The energy level diagram of dual CARS is presented in Figure 1D. The CARS signal created by the two Stokes pulses, probing IFDs in the finger print region, is not detected in the present set-up.

2.2 | Samples

2.2.1 | Beads

The sample was prepared by pipetting 10 μL of 1% solid suspension of 20 μm diameter polymethyl methacrylate (PMMA) beads (MMA20K, Phosphorex) and 10 μL of 1% solid suspension of 10 μm diameter polystyrene (PS) beads (118, Phosphorex), onto a glass coverslip (#1.5, 24 × 50 mm, Thermo Scientific), and mixing them before covering with a further glass coverslip and sealing the edges with an adhesive coating (OP-4-20641, Dymax).

2.2.2 | Reverse emulsion

A sample containing heavy water (99% purity, Sigma Aldrich), water and olive oil (mechanically extracted extra virgin olive oil with mostly oleic acid) was prepared. Dishwashing liquid (Hand Dishwash, Neutral) was added to 1 mL olive oil at 0.1% v:v as surfactant. To prepare a reverse emulsion, 0.5% v:v of water was added, and the sample was vigorously shaken by hand in a test tube for 30 s before adding 0.5% v:v of heavy water and shaking the tube again for 30 s. Ten microlitres of the emulsions

was pipetted onto a glass coverslip (#1.5, 24 × 25 mm, Thermo Scientific) before covering the sample with another glass coverslip. The surfactant is stabilising the small water droplets, hindering their coalescence.

2.2.3 | Deuterated HeLa cells

Deuterated lipids in fixed human cervical carcinoma (HeLa) cells were prepared by using the protocol of Ref. [20]. The cells (ATCC) were cultured in minimum essential medium (MEM) supplemented with GlutaMAXTM (Life Technologies), 10% (v:v) foetal bovine serum (FBS) (Life Technologies), 1× Non-Essential Amino Acids (Life Technologies) and 1 mM sodium Pyruvate (Life Technologies) directly onto glass coverslips (thickness #1.5, 25 mm diameter, VWR). Following overnight attachment, cells were transferred to MEM containing supplements and a complex of bovine serum albumin (BSA) (Sigma Aldrich) and the investigated fatty acid at a concentration of 47 µg/mL. Fatty acid–BSA complexes were formed by adapting a published protocol, which involved combining 5% BSA/PBS solutions with 20 mM sodium–fatty acid solutions to form fatty acid–BSA complexes with a final concentration of 1.656 mg/mL. Following an 18-h incubation period in fatty acid–BSA–supplemented media, coverslips were fixed in a 4% formaldehyde–PBS solution (Affymetrix) for 20 minutes and mounted onto standard glass microscope slides using a 13 mm hole diameter, 120-µm-thick adhesive imaging gasket (Grace BioLabs) filled with water containing Anti-Anti (Life Technologies).

3 | RESULTS

3.1 | Beads

To demonstrate the absence of motion artefacts in dual CARS, a sample containing flowing PS and PMMA beads (see Section 2.2.1) was measured. The pump and tunable Stokes beam were set to 827 and 1093 nm centre wavelength, respectively, and to 20 mW power each at the sample. By adjusting the delay line, the IFD was set to about 3050 cm^{-1} where the PS vibrational resonance provides strong CARS while CARS from PMMA is suppressed due to the destructive interference of resonant and non-resonant contributions.[12] The fixed Stokes beam was also set to 20 mW and its IFD to about 2336 cm^{-1}, non-resonant for both PMMA and PS. Acquiring both CARS signals simultaneously allows to colour code the beads without having motion artefacts even when the beads are moving. An image illustrating artefact-free imaging of a dynamic sample is presented in Figure 2. The 20 µm PMMA beads have a dominant S_{SR} shown in the green colour, while their signal in S_{CH} shown in the red colour is suppressed as expected. Conversely, the 10 µm PS bead is appearing red due to the strong S_{CH} with S_{SR} being much weaker. The two bead materials are thus well separated by the dual CARS. To exemplify the flow dynamics of the beads, a time sequence with 1 s time step is shown for a selected region. Clearly, the beads are moving significantly, with a speed of a few microns per second, without creating motion artefacts in the chemical assignment seen by the colour.

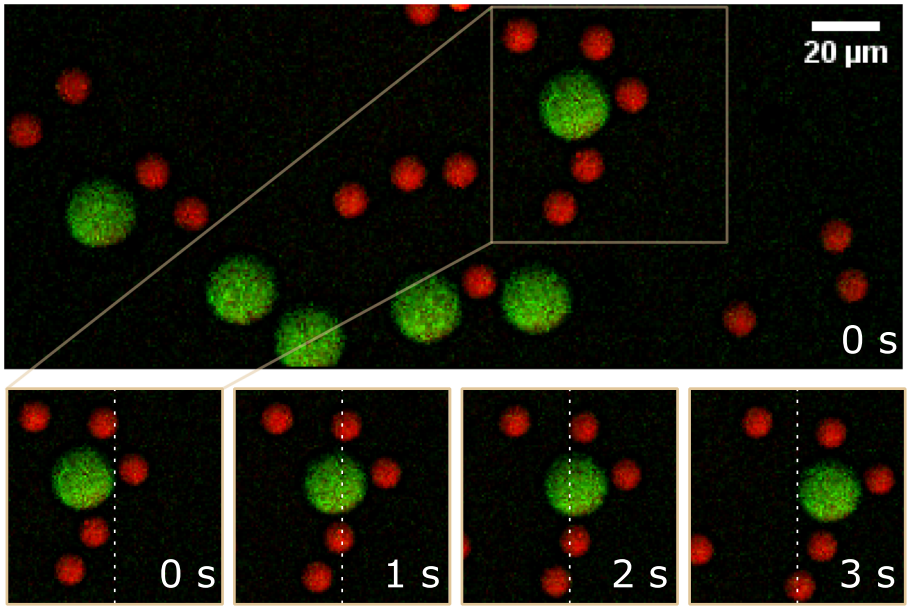

FIGURE 2 CARS images of flowing PS (10 µm diameter) and PMMA (20 µm diameter) beads, using an RGB colour overlay, taken with 0.5 s frame time, 400 × 400 pixels and 3.125 µs pixel dwell time. The green colour shows the signal S_{SR} on a scale from 0 to 0.98 V (0–6 × 10^7 photoelectrons/s, 0–188 photoelectrons over dwell time) and is strongest for the PMMA beads. The red colour shows S_{CH} on a scale 0–15 counts and is dominated by the PS beads. The bottom images show a time course of a selected area as indicated with 1 s intervals to exemplify the flow. The white dashed line is for motion reference.

3.2 | Reverse emulsion

To demonstrate the imaging of a three-component mixture with resonances in the silent region, a sample containing an oil, water and heavy water reverse emulsion (see Section 2.2.2) was measured. To target water, deuterated water and oil vibrational frequencies, the pump beam was tuned to 831 nm to address with the fixed Stokes beam the deuterated water C–D stretch[21] at 2400 cm^{-1}. Both delay lines were calibrated according to the procedure described in Appendix C. An example of a resulting S_{SR} image is given in Figure 3A. Simultaneously, the pump and the variable Stokes beam at 1110 nm were addressing a minimum of the oil signal at 3080 cm^{-1} due to the destructive interference of the resonant signal and the non-resonant background.[21] The resulting S_{CH} is shown in (B) and combined with (A) in the red–blue colour overlay in (C). The variable Stokes beam and the delay line were then tuned to 1072 nm to address the oil resonance at 2850 cm^{-1}, and the resulting simultaneously acquired S_{SR} and S_{CH} are given in (D) and (E), respectively, with a red–green colour overlay shown in (F). Using all three IFDs measured, the overlay of (A) in red, (B) in blue and (E) in green shown in (G) clearly identifies the three different materials. Interestingly, not only water droplets but also a water vesicles can be seen, stabilised by the surfactant. The advantage of having two-variable wavelength beams with one fixed wavelength beam is the ability to distinguish three different materials with two independent scans.

3.3 | Deuterated human cervical carcinoma cells

Dual CARS imaging capabilities were tested by imaging deuterated lipids in fixed human cervical carcinoma (HeLa) cells which were prepared as detailed in Section 2.2.3. The HeLa cells were imaged with the pump at 831 nm and the tuneable Stokes at 1093 nm to address the non-deuterated lipid region, while using the fixed Stokes at 1025 nm for the deuterated lipid region. The power at the sample was 27 mW for the pump, 18 mW for the tunable Stokes and 16 mW for the fixed Stokes beams. A sequence of 20 images of 4000×4000 pixels with 3.75 µs pixel dwell time was taken at different IFDs by moving both delay lines by 62.5 µm steps between images, corresponding to 29 cm^{-1} IFD shift per step. The final images were rescaled to 368×368 image size by pixel binning and are presented in Figure 4. The spectra averaged over a selected lipid droplet (see squares Figure 4B,D) showing signal from deuterated lipids are presented in Figure 4A for the C–H signal S_{CH} and in Figure 4C for the C–D signal S_{SR}. CARS spectra of deuterated lipids are given in Boorman et al,[21] showing vibrations across the region 2070–2200 cm^{-1}.

The ratio between the signal at droplets and away from droplets is shown as black line—featuring the typical dispersive shape of a weak resonance in CARS. In order to isolate lipid contrast, images I_1 and I_2 at two IFDs, indicated by the vertical dashed lines, have been selected and their weighted difference $I_\Delta = I_1 - \alpha I_2$ using a weight α has been calculated to provide contrast for the lipid droplets both in the C–H and C–D range. Images in Figure 4B,D show these spectrally unmixed data, using $\alpha = 0.62$ for the C–H region and $\alpha = 0.73$ for the C–D region to match the mode of the image values before subtraction. Colour overlays of αI_2 and I_Δ image are also shown.

From the I_Δ images, it can be observed that the set-up is sensitive to deuterated lipids which are imaged simultaneously with the regular lipids inside HeLa cells. The CARS signal from the deuterated lipid region is weak due to small amount of C–D bonds in the sample.

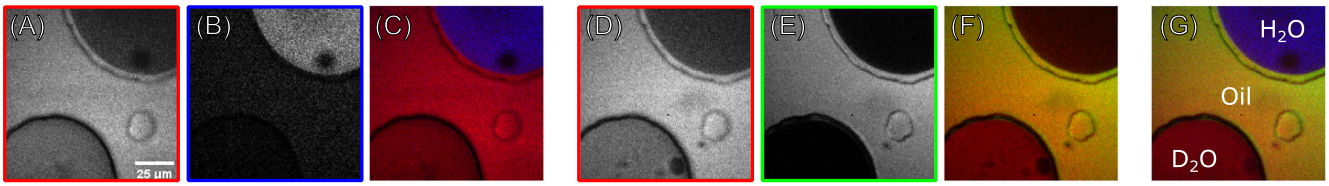

FIGURE 3 CARS imaging on an oil/water/deuterated water reverse emulsion showing water droplets inside oil. Images (A) and (D) show S_{SR} at 2400 cm^{-1} resonant to the C–D stretch of deuterated water, on a scale from 0 (black) to 0.68 V (white) (4.3×10^7 photoelectrons/s, 0–538 photoelectrons per dwell time). (B) shows S_{CH} obtained simultaneously with (A), addressing the minimum of the oil CARS signal at 3080 cm^{-1}, on a scale from 0 to 25 counts. (C) is an RGB colour overlay with (A) in the red and (B) in the blue colour. (E) shows S_{CH} at 2850 cm^{-1} providing the highest CARS signal of oil, on a scale from 0 to 100 counts and is obtained simultaneously with (D). (F) is an overlay with (D) in the red and (B) in the green colour. (G) is a combined overlay of (A) in red, (B) in blue and (E) in the green colour, revealing water in blue, deuterated water in red and oil in yellow. Frame time was 2 s with 400×400 pixels and 12.5 µs pixel dwell time. Pump and fixed Stokes beam power was set to 20 mW while the variable Stokes power was set to 15 mW.

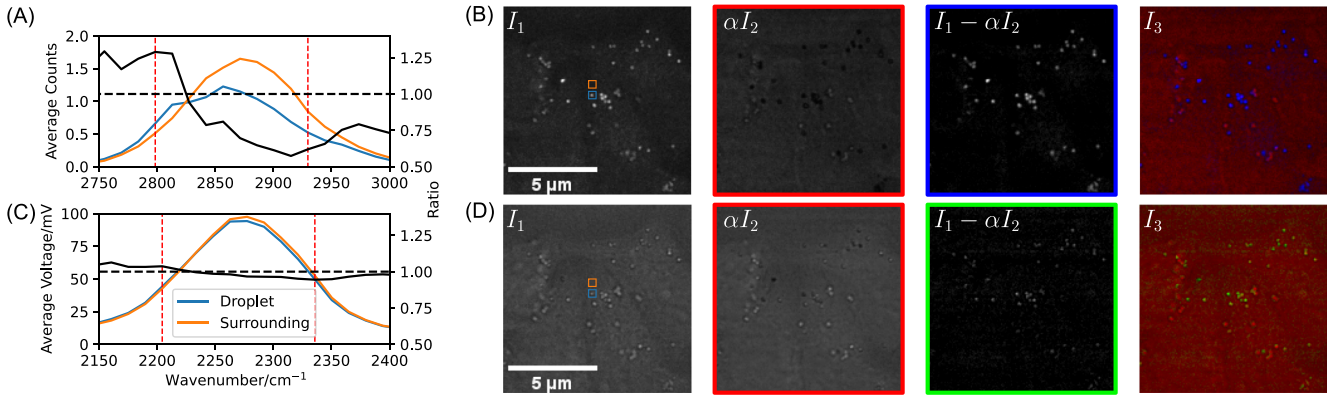

FIGURE 4 Deuterated lipid droplets in fixed HeLa cells imaged with dual CARS. Frame time was 60 s with 4000 × 4000 pixels and 3.75 µs pixel dwell time. The images were scaled to 368 × 368 pixels. The average signal over a 6 × 6 pixel square of a droplet (blue) or its surrounding (orange) of S_{CH} (A) and S_{SR} (C) are given as solid lines, with the ratio droplet to surrounding given as black line. The vertical red dashed lines indicate the spectral positions of the images I_1 and αI_2 shown in (B) and (D), with $\alpha = 0.62$ and $\alpha = 0.73$, respectively. Greyscale black to white over 0 to 5 counts in (B) and 0 to 0.22 V (1.4×10^7 photoelectrons/s) in (D). $I_\Delta = I_1 - \alpha I_2$ is shown in 8-bit greyscale, and the colour-coded images I_3 to the right are overlays of αI_2 in red and I_Δ in blue (B) and green (D).

4 | CONCLUSIONS

In this work, we have demonstrated dual CARS microscopy using a single femtosecond laser source and spectral focusing to image the cell-silent region and C–H stretch vibrational region simultaneously. This simplifies the setup compared with previous systems using two separate sources.[17,18] The system allows the imaging of deuterated (C–D) and non-deuterated (C–H) organic materials without motion artefacts. The GDD control inside the source allows to fine adjust the spectral focusing and also to apply negative group delay to achieve Fourier-limited femtosecond pulse durations for second and third harmonic generation imaging, allowing for multimodal imaging with a single source.

AUTHOR CONTRIBUTIONS

Dominykas Gudavičius: Methodology (supporting); software (supporting); validation (lead); formal analysis (lead); investigation (lead); resources (equal); data curation (lead); writing—original draft (equal); writing—review and editing (equal); visualisation (lead). **Lukas Kontenis**: Methodology (supporting); software (lead); writing—review and editing (supporting); supervision (supporting); project administration (equal). **Wolfgang Langbein**: Conceptualisation (lead); methodology (lead); software (supporting); validation (supporting); resources (equal); writing—original draft (equal); writing—review and editing (equal); visualisation (supporting); supervision (lead); project administration (equal); funding acquisition (supporting).

ACKNOWLEDGMENTS

We wish to acknowledge Iestyn Pope and Pete Watson (Cardiff University) for providing reference samples and deuterated cell samples, Jonas Berzinš (Light Conversion) for proofreading and commenting on the draft and Paola Borri for support. This project has received funding from the European Union's Horizon 2020 research and innovation programme under the Marie Skłodowska-Curie Grant Agreement No. 812992.

CONFLICT OF INTEREST STATEMENT

The authors declare no potential conflict of interests.

DATA AVAILABILITY STATEMENT

Information about the data created during this research, including how to access it, is available from Cardiff University data archive (https://doi.org/10.17035/d.2023.0290258940).

ORCID

Dominykas Gudavičius https://orcid.org/0009-0003-9846-9412
Lukas Kontenis https://orcid.org/0000-0002-8856-9538
Wolfgang Langbein https://orcid.org/0000-0001-9786-1023

REFERENCES

[1] A. Zumbusch, W. Langbein, P. Borri, *Prog. Lipid Res.* **2013**, *52*, 615.
[2] C. Zhang, D. Zhang, J.-X. Cheng, *Annu. Rev. Biomed. Eng.* **2015**, *17*, 415.

[3] C. Zhang, J. A. Aldana-Mendoza, *J. Phys. Photonics* **2021**, *3*, 32002.
[4] H. Lin, J.-X. Cheng, *eLight* **2023**, *3*, 1.
[5] L. Gong, W. Zheng, Y. Ma, Z. Huang, *Nat. Photonics* **2019**, *14*, 115.
[6] E. M. Vartiainen, H. A. Rinia, M. Müller, M. Bonn, *Opt. Express* **2006**, *14*, 3622.
[7] Y. Liu, Y. J. Lee, M. T. Cicerone, *Opt. Lett.* **2009**, *34*, 1363.
[8] F. Masia, A. Glen, P. Stephens, P. Borri, W. Langbein, *Anal. Chem.* **2013**, *85*, 10820.
[9] C. L. Evans, E. O. Potma, X. S. Xie, *Opt. Lett.* **2923**, *2004*, 29.
[10] W. Langbein, D. Regan, I. Pope, P. Borri, *APL Photonics* **2018**, *3*, 92402.
[11] F. Ganikhanov, C. L. Evans, B. G. Saar, X. S. Xie, *Opt. Lett.* **2006**, *31*, 1872.
[12] I. Rocha-Mendoza, W. Langbein, P. Watson, P. Borri, *Opt. Lett.* **2258**, *2009*, 34.
[13] I. Pope, W. Langbein, P. Watson, P. Borri, *Opt. Express* **2013**, *21*, 7096.
[14] L. Li, H. Wang, J.-X. Cheng, *Biophys. J.* **2005**, *89*, 3480.
[15] C. Di Napoli, F. Masia, I. Pope, C. Otto, W. Langbein, P. Borri, *J. Biophotonics* **2014**, *7*, 68.
[16] B. Sarri, X. Chen, R. Canonge, S. Grégoire, F. Formanek, J.-B. Galey, A. Potter, T. Bornschlögl, H. Rigneault, *J. Controlled Release* **2019**, *308*, 190.
[17] O. Burkacky, A. Zumbusch, C. Brackmann, A. Enejder, *Opt. Lett.* **2006**, *31*, 3656.
[18] R. Mouras, G. Rischitor, A. Downes, D. Salter, A. Elfick, *J. Raman Spectrosc.* **2010**, *41*, 848.
[19] K. Hiramatsu, T. Tajima, K. Goda, *ACS Photonics* **2022**, *9*, 3522.
[20] L. L. Listenberger, D. A. Brown, *Curr. Protoc. Cell Biol.* **2007**, *35*(1), 24.
[21] D. Boorman, I. Pope, F. Masia, P. Watson, P. Borri, W. Langbein, *J. Raman Spectrosc.* **2021**, *52*, 1540.
[22] C. A. Klein, *Appl. Opt.* **1986**, *25*, 1873.
[23] I. Rocha-Mendoza, W. Langbein, P. Borri, *Appl. Phys. Lett.* **2008**, *93*, 201103.
[24] W. Langbein, I. Rocha-Mendoza, P. Borri, *J. Raman Spectrosc.* **2009**, *40*, 800.

How to cite this article: D. Gudavičius, L. Kontenis, W. Langbein, *J Raman Spectrosc* **2024**, 1. https://doi.org/10.1002/jrs.6671

APPENDIX A: DISPERSION BLOCK REFRACTIVE INDEX

In this work, blocks made of heavy flint glass SF57 and N-SF66, or ZnS crystals were used. The refractive index of the glass was expressed by the Sellmeier equation:

$$n^2(\lambda) = 1 + \sum_{i=1\ldots3} \frac{B_i}{1 - C_i/\lambda^2}, \tag{A1}$$

with the light wavelength λ in vacuum, and the Sellmeier coefficient values given in Table A1. For ZnS, we used instead the expression[22]

$$n^2(\lambda) = \epsilon_0 + \frac{A}{\lambda^2 - {\lambda_U}^2} + \frac{\epsilon_0 - \epsilon_\infty}{\lambda^2/{\lambda_I}^2 - 1}, \tag{A2}$$

with $\epsilon_0 = 8.393$, $\epsilon_\infty = 5.105$, $\lambda_U = 0.2421\,\mu m$, $\lambda_I = 36.71\,\mu m$ and $A = 0.14383\,\mu m^2$.

APPENDIX B: SPECTRAL FOCUSING

Vibrational resonances in typical biological samples have linewidths in the 10–50 cm^{-1} range, corresponding to vibrational coherence times in the picosecond range. Achieving such spectral resolution accordingly requires excitation and probing pulse duration in the picosecond range. As the source used in the present work delivers 100–200 fs pulses, we implemented spectral focusing for better resolution and faster tuning speed[23,24] to stretch the pulses by the dispersion of the refractive index $n(\lambda)$ in optical media. Assuming Gaussian pulses of electric field $E(t) = \frac{1}{2}\mathcal{E}(t)\exp(i(\omega_0 + \beta t)t) + \text{c.c}$ where $\mathcal{E}(t)$ is the Gaussian-shaped carrier envelope and c.c is the complex conjugate, the instantaneous frequency is given by $\omega(t) = \omega_0 + 2\beta t$ where β is the linear chirp parameter. To achieve a Fourier-limited spectral resolution in the vibrational frequency, the linear chirp parameters of all three pulses must be the same, yielding a constant IFD. In this work, blocks of heavy flint glass SF57 and N-SF66 and ZnS were added to the set-up, having a refractive index dispersion $n(\lambda)$ as given in Appendix A. This introduces a group delay dispersion

$$g = \sum_i \frac{\lambda^3}{2\pi c^2} \frac{d^2 n_i}{d\lambda^2} L_i, \tag{B1}$$

where c is the speed of light in vacuum and L_i is the block length and the sum runs over all blocks traversed. The resulting linear chirp parameter is given by

$$\beta = \frac{g}{\pi c\left(g^2 + t_0^4/(4\ln 2)^2\right)}, \tag{B2}$$

where t_0 is the intensity FWHM of the unchirped pulse and the corresponding chirped pulse duration is

$$t_f = t_0\sqrt{1 + \left(\frac{4g\ln 2}{t_0^2}\right)^2}. \tag{B3}$$

To visualise the applied chirp and to relate the time and frequency domain, the Wigner–Ville distribution for a $t_0 = 150$ fs pulse centred at 1025 nm, before and after stretching to $t_f = 1300$ fs, is given in Figure 1C. The spectral resolution calculated by taking the geometric mean of individual pulse resolutions[24] is 14.7 cm^{-1} for the pump and variable Stokes beams and 15.5 cm^{-1} for the pump and fixed Stokes beam. Using spectral focusing, different resonant frequencies can be addressed by changing the pump–Stokes pulse delay, as discussed in Ref. [24]. To calibrate the IFD versus delay line position, we used reference samples with well-defined vibrational resonances, as detailed in Appendix C.

TABLE A1 Coefficients of the Sellmeier dispersion for the glass used for spectral focusing.

Material	SF57	N-SF66
B_1	1.82	2.02
B_2	0.43	0.47
B_3	1.07	2.60
$C_1/\mu m^2$	0.014	0.015
$C_2/\mu m^2$	0.060	0.069
$C_3/\mu m^2$	121.52	161.82

APPENDIX C: OPTICAL DELAY TO IFD CALIBRATION

The delay line calibration relating displacement to wavenumbers is required to establish the IFD used for a given measurement. It was performed by homogeneous material calibration samples. For the silent region, we used 4-nitrophenylacetonitrile (>98%, Sigma Aldrich) having a well-distinguished peak at 2251 cm^{-1}. A small amount of the powder was put on a microscope slide and heated on a hotplate to 130°C until fluid, then covered with a

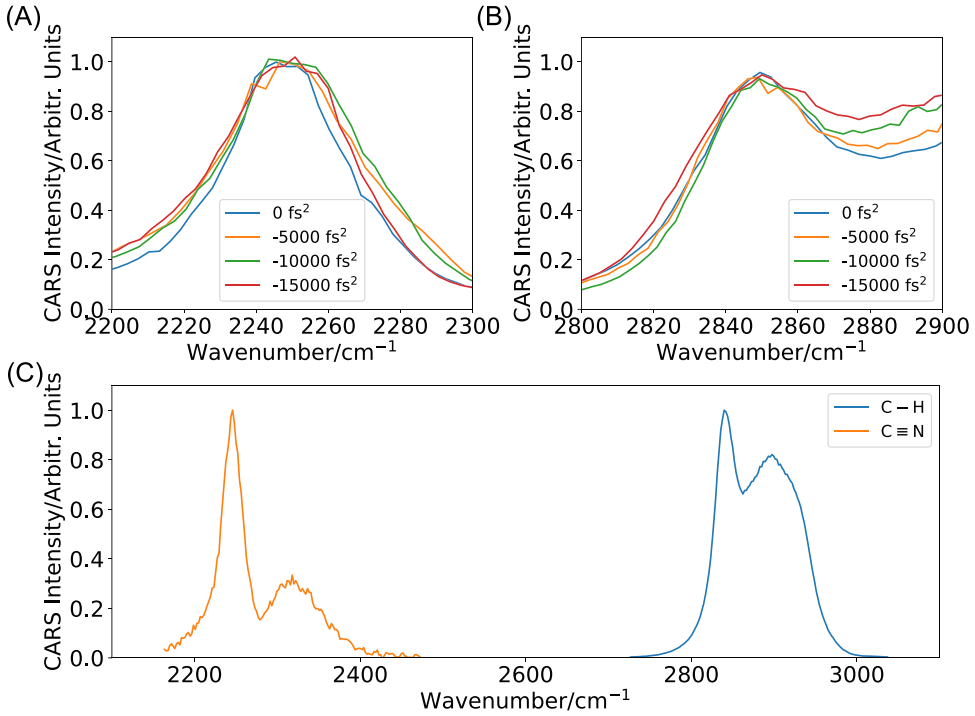

FIGURE B1 Spectral focusing chirp matching and calibration. CARS intensity versus delay calibrated as IFD using the pump at 831 nm and different GDD settings of the CRONUS-2P as indicated. (A) cell-silent region (S_{SR}) on 4-nitrophenylacetonitrile with a peak at 2251 cm^{-1} using the fixed Stokes at 1025 nm and 2 mW of pump and Stokes at the sample. (B) C–H region (S_{CH}) on oil with a peak at 2850 cm^{-1} using the variable Stokes at 1100 nm and 10 mW of pump and Stokes at the sample. (C) CARS on calibration samples as in (A) and (B) at zero GDD of the CRONUS-2P over the full spectral range.

coverslip, removed from the hotplate and sealed with nail varnish after cooling. For the C–H stretch region, we used olive oil (mechanically extracted extra virgin olive oil) with a peak at 2850 cm^{-1}. A small drop of olive oil was placed on a coverslip, covered with a second coverslip and sealed with nail varnish (Buk, Editcosmetics). For the C–H channel, pump and variable Stokes beams were set to the wavenumbers for which the calibration is required and the power per beam was set to 10 mW. The dwell time was set to 50 ms, and for PMT1, a 50 kHz filter (EF124, Thorlabs) was used. The delay line was moved in steps of 12.5 µm across the region of pulse overlap.

A CARS optical delay scan at fixed pump and Stokes wavelengths on the calibration samples produces a spectrum with a well-distinguished peak. The linear chirp parameter β of the spectral focusing was calculated using Equation (B2) and the lengths and materials provided before, resulting in $2\beta = 0.07$ cm^{-1}/fs for the pump and Stokes beams. To fine-tune the linear chirp parameter for best spectral resolution, the GDD control of the CRONUS-2P was used to minimise the spectral feature width, thereby adjusting the pump to match the fixed Stokes for the silent region, and the tuneable Stokes to match the pump for the C–H stretch region. CARS spectral peak shapes of the calibration samples for different GDD settings are presented in Figure B1, showing in (A) the 4-nitrophenylacetonitrile peak at 2251 cm^{-1} and in (B) the oil peak at 2850 cm^{-1}. For the silent region calibration, the pump and Stokes power was reduced to 2 mW to avoid sample damage. We can clearly observe the change of the peak width depending on the GDD setting. The narrowest peak is achieved at zero GDD setting, as expected. Because the optical delay p_p at the spectral peak and the corresponding peak position in wavenumbers ν_p is known, we can convert any optical delay p into wavenumbers using $\nu = \nu_p + 2\beta(p - p_p)$. The resulting spectra of the calibration samples are shown in Figure B1C.